Precambrian Research 224 (2013) 23–35

Contents lists available at SciVerse ScienceDirect

Precambrian Research

journal homepage: www.elsevier.com/locate/precamres

Hydrothermal activity during Ediacaran–Cambrian transition: Silicon isotopic evidence

Haifeng Fan[a,b,*], Hanjie Wen[a], Xiangkun Zhu[b], Ruizhong Hu[a], Shihong Tian[c]

[a] State Key Laboratory of Ore Deposit Geochemistry, Institute of Geochemistry, Chinese Academy of Sciences (CAS), Guiyang 550002, China
[b] Institute of Geology, Chinese Academy of Geological Sciences (CAGS), Beijing 100037, China
[c] Institute of Mineral Resources, Chinese Academy of Geological Sciences (CAGS), Beijing 100037, China

ARTICLE INFO

Article history:
Received 19 January 2012
Received in revised form 16 August 2012
Accepted 5 September 2012
Available online 18 September 2012

Keywords:
Ediacaran–Cambrian transition interval
Bedded chert deposits
Si isotope
Hydrothermal activity

ABSTRACT

Abundant bedded chert deposits occurred at the Ediacaran–Cambrian transition interval at the Yangtze Platform, South China. However, there is not a non-controversial and integrated model for the origin of these chert deposits from trace element patterns and oxygen isotopic evidence. To understand the origin and the oceanic environment of these chert deposits, we analyzed the Si isotopic composition, major and trace elements of chert samples from two stratigraphically correlated sections with a depositional age around 542 Ma. The relationship between Al_2O_3 content and Si isotopic values indicated three end-member sources of Si derivation. The most negative δ^{30}Si values (−0.3‰ to −0.5‰) reflect the silicon derived from hydrothermal fluids due to intense tectonic activity. The most positive δ^{30}Si values (up to +1.2‰) could reflect the increase of ^{30}Si in the hydrothermal fluid by precipitation, or the signature of seawater. The medium δ^{30}Si value (+0.2‰ to +0.7‰) could be interpreted as the mixing of the hydrothermal fluid and volcanic materials with negative δ^{30}Si and ambient seawater with positive δ^{30}Si. It is obvious that the injection of Si-rich hydrothermal fluid would affect the δ^{30}Si and trace element distribution of seawater. In addition, we estimated that the δ^{30}Si values of Ediacaran–Cambrian transitional seawater range from +2.2‰ to +3.5‰ based on assumed fractionation factors $-2.3‰ < \varepsilon < -1.0‰$ between precipitated Si in chert deposits and initial dissolved Si in seawater. According to Si isotopic composition and other geochemical evidence, we maintain that hydrothermal activity played an important role not only in the formation of bedded chert and polymetallic ore deposits, but also in the oceanic environment and concurrent evolution of life during Ediacaran–Cambrian transition interval.

1. Introduction

The Ediacaran–Cambrian (E–C) transition was a critical time interval for understanding these simultaneous events: the further increase of atmospheric oxygen, the rapid increase in the abundance and diversity of biomass, the prolonged global oceanic anoxia, the major plate tectonic reconfigurations and the extensive anorogenic volcanism (Kirschvink et al., 1997; Veevers et al., 1997; Doblas et al., 2002). Although there are extensive studies about remarkable biological, oceanic and geochemical changes across the E–C transition, the triggering mechanism of these concurrent issues still remains controversial.

During the transitional interval, widespread bedded chert successions occurred at the slope to deep-water basin around both the northern and the southern margins of the Yangtze Platform, South China (Chen et al., 2009). Also present are massive barite deposits associated with these cherts and Ni–Mo–PGE polymetallic ore horizons within host black shales that overlie these cherts (Lott et al., 1999; Steiner et al., 2001; Jiang et al., 2003). Numerous studies on the polymetallic ores and barite deposits were carried out and different genetic models were proposed as hydrothermal model (Steiner et al., 2001; Jiang et al., 2003) and seawater origin model (Mao et al., 2002). However, the origin of these chert deposits at the E–C boundary were poorly constrained, although both hydrothermal (Li and Gao, 1996; Li, 1997; Peng et al., 1999) and marine (biogenic) origins (Guo et al., 2007; Chang et al., 2008) have been proposed as well. Even though poorly constrained, these chert deposits contain unique information of the ambient surface environment in early Earth history, and deserve further study. However, the relationship between these cherts and oceanic environmental change still remains subject to debate. Therefore, the origin of these cherts could be of significance in solving these controversies.

Recently some authors attempted to trace the origin of Archean cherts and the environment of the Early Archean Ocean by using

* Corresponding author at: State Key Laboratory of Ore Deposit Geochemistry, Institute of Geochemistry, Chinese Academy of Sciences (CAS), Guiyang 550002, China. Tel.: +86 851 5895037.
E-mail address: tonyfanhaifeng@gmail.com (H. Fan).

0301-9268/$ – see front matter © 2012 Elsevier B.V. All rights reserved.
http://dx.doi.org/10.1016/j.precamres.2012.09.004

silicon isotopes (Robert and Chaussidon, 2006; Van den Boorn et al., 2007, 2010; Carbonne et al., 2011; Abraham et al., 2011). Based on the fractionation of silicon isotope under near surface conditions, hydrothermal fluid could be considered as an important contributor to those cherts (Carbonne et al., 2011), but Robert and Chaussidon (2006) clearly stated that there is no significant temperature effect on Si isotopic fractionation between precipitated and dissolved silicon. Recently, hydrogen and oxygen isotopic data (Hren et al., 2009; Blake et al., 2010) argued for oceanic temperature invariability from the Archean to Cambrian. Even with this variability in temperature, Van den Boorn et al. (2007) inferred that the Si isotope variability in a suite of 3.5–3.0 Ga cherts reflects different sources of silicon. However, there is little study about Si geochemical cycling during the E–C transitional interval. Only Peng et al. (1999) and Jiang and Li (2005) reported significant variation of the Si isotopic composition of a few cherts from Yangtze Platform at the E–C boundary, providing insights into the silicon cycle at this time. From a correlation between $\delta^{30}Si$ and $\delta^{18}O$ values in a few cherts, they have estimated a higher oceanic temperature (80 °C) which suggested hydrothermal activity.

To better understand Si isotopic signatures as a tracer for the origin of widespread bedded chert deposits, contemporaneous oceanic environmental change, and the origin of metallic ore deposits during E–C transitional interval, we studied two representative sections of well characterized cherts (about 551–532 Ma) and other inter-bedded sample types from the Yangtze Platform. Not only Si isotopes, but also mineralogy, major and trace element geochemical signatures were investigated in this paper in order to model the origin of chert deposits and to illustrate the relationship among these chert deposits, oceanic environmental change and polymetallic ore deposits.

2. Geological setting

During the E–C transitional interval, there are four different sedimentary facies distinguished in South China, including a shallow-water carbonate platform, a protected basin, the Jiangnan uplift and a deep-water basin, as illustrated in Fig. 1A (Steiner et al., 2001; Wang and Li, 2003). In several areas, they are exposed across a transition zone from platform to basin, offering an opportunity to investigate the stratigraphic features during this critical interval of Earth history, which can provide insight into sea-level fluctuations, oceanic anoxia, metal accumulation and the corresponding ocean–atmosphere–biosphere evolution (Guo et al., 2007).

Two stratigraphic sections were selected for this study, the Chuanyanping section in Hunan province and the Yinjiang section in Guizhou province, which are separated from each other by 240 km. These two sections were palaeogeographically located along the southern marginal zone of the Yangtze Platform (Guo et al., 2007; Chen et al., 2009). The southern marginal zone of the Yangtze Platform was extended approximately along the antecedent Jinningian (−0.8 Ga) orogenic zone between the Yangtze Block and Cathaysia Block (Li, 1999; Zheng et al., 2008) (Fig. 1A).

The Chuanyanping section crosses the E–C boundary. It includes the upper part of the Ediacaran Doushantuo and the Dengying Formation and the lower part of Cambrian Niutitang Formation, representing a shallow shelf depositional environment. The major lithofacies of the Dengying Formation is gray carbonates. The lower Cambrian Niutitang Formation consists of black-gray cherts and an upper thick black shale succession (up to 100 m thick) (Fig. 1B) composed mostly of a basal Ni–Mo–PGE sulfide-rich horizon (Steiner et al., 2001). The thickness of the chert was dependant on the distance from Dayong-Cili fault. The fault plays an important role in controlling metallogenesis of Ni–Mo–PGE sulfide layer (Li, 1997). In the region, one SHRIMP U–Pb zircon age has been obtained, 536.3 ± 5.5 Ma for the tuff layer overlying the chert deposit of the Liuchapo Formation from Ganziping section (Chen et al., 2009), which is equivalent to the E–C boundary age (542 Ma).

The Yinjiang section is located in a slope to basinal setting and includes the Doushantuo Formation composed of black shales, overlain by the Liuchapo Formation composed of black cherts, and the thick black shale of Jiumengchong Formation (Fig. 1B), all representing slope deposition. The Jiumengchong Formation is equivalent to the Niutitang Formation for which Jiang et al. (2009) reported the SHRIMP U–Pb zircon age, 532 ± 0.7 Ma, for the basal tuff layer of the Niutitang Formation in Zunyi area. Bivalved arthropods (*Sunella*) and tubular fossils (*Sphenothallus*) have been found in the black shales of the lower part of Jiumengchong Formation only several kilometers away from the Yinjiang section (Yang et al., 2003).

3. Sampling and analytical methods

3.1. Sample description

Samples were collected from the Yinjiang section of Northeast Guizhou province and the Chuanyanping section of western Hunan province, South China (Fig. 1). In the laboratory, samples were washed with distilled water and dried at 80 °C, and then crushed into powder (−200 mesh).

In these studied cherts, the crystal size of quartz tends to be quite variable, from several μm to several hundred μm. Individual quartz crystals have irregular crenulate crystal boundaries and a pronounced undulose extinction (Fig. 2A and B) similar to typical micro-crystalline and meso-crystalline quartz, which results from the disordered crystallographic structure of individual grains (Knauth, 1994). The meso-crystalline quartz (20–50 μm) is the most common recystallized quartz phase in chert samples. Large pores and cavities within these chert samples are commonly filled with length-fast mega-crystalline quartz, and there are also a few quartz veins (Fig. 2C and D), and only minor carbonate minerals (Fig. 2D).

3.2. Methods

The major elements were determined by X-ray fluorescence (XRF) using lithium tetraborate powder pelleting at the ALS Chemex (Guangzhou) Co., Ltd. The standard reference materials (SRM) were analyzed together with unknown samples and suggested that the precision is better than 5%. The trace elements were analyzed by Inductively Coupled Plasma Mass Spectrometry (ICP-MS) in the Institute of Geochemistry, CAS. The precision is better than 3%, which is calculated from the results of standard reference materials such as GBPG-1 (Garnet-Biotite Plagiogneiss), OU-6 (Penrhyn Slate) and AMH-1 (Mount Hood Andesite) (Qi et al., 2000).

The method for measuring Si isotopes was detailed in Ding et al. (2004, 2008). For measurement of Si isotopic composition, the carbonate must be removed by batching with HCl and organic fractions were removed by heating at high temperature (500 °C). After these fractions were removed the SiO_2 was reacted with BrF_5 in a metal vacuum line to form SiF_4. First, the SiF_4 was separated from O_2, N_2, BrF_3 and BrF_5 by cryogenic separation at the dry ice acetone and liquid nitrogen temperatures. Subsequently the SiF_4 gas was purified by transfer through a Cu tube containing pure Zn particles at 60 °C. All the Si isotopic compositions were analyzed with a MAT-253 gas source isotope ratio mass-spectrometer in the Institute of Mineral Resources, CAGS. The silicon isotope ratios were measured using a single collector by the peak jumping method. Two Chinese national reference materials (GBW04421 and GBW04422, Ding et al., 2004,

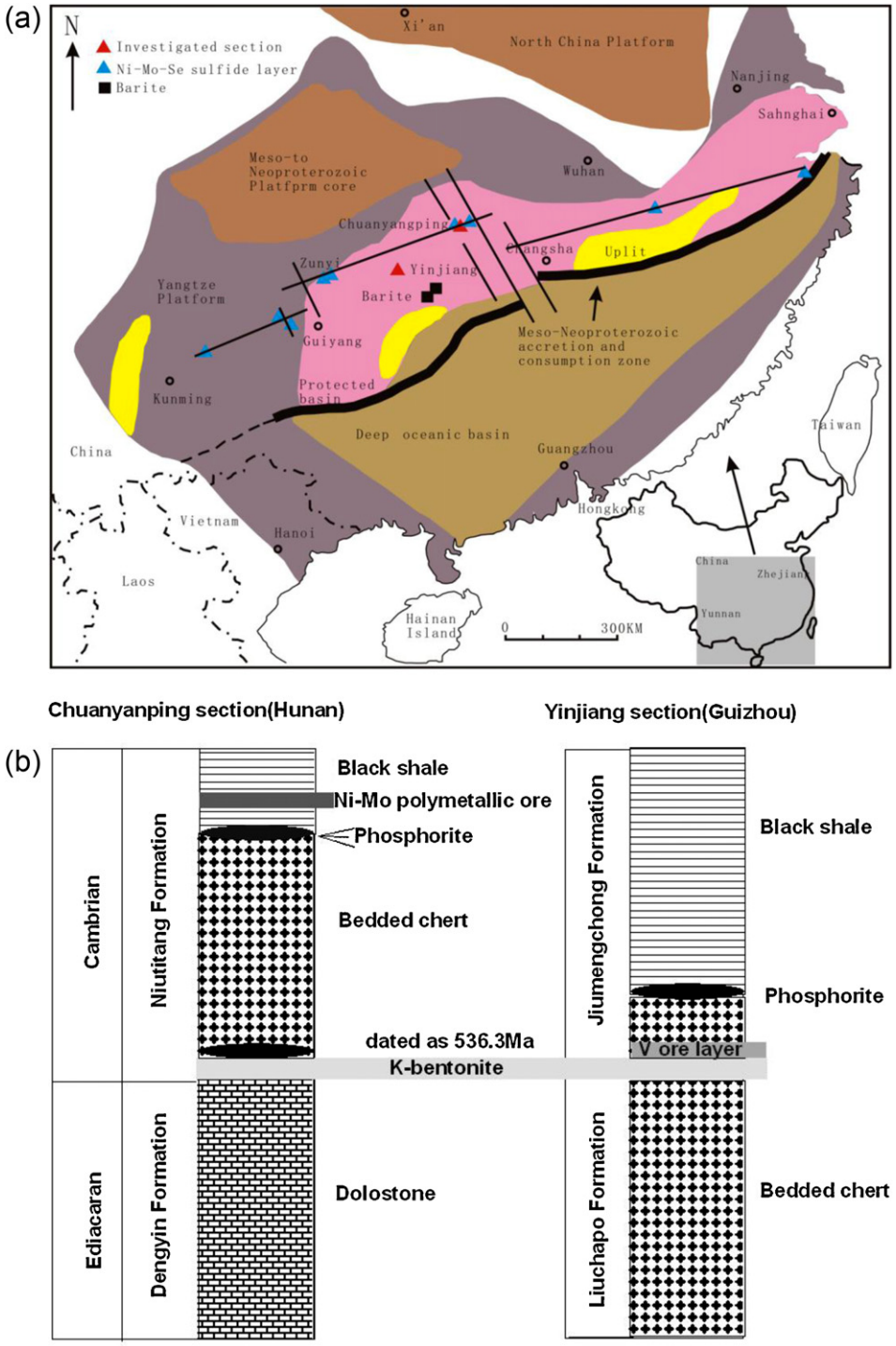

Fig. 1. (a) Simplified palaeogeographic map of the Yangtze Platform during Ediacaran–Cambrian transition modified from Steiner et al. (2001). Note the distribution of bedded chert from Early Cambrian and Late Ediacaran straigraphic successions. The two red triangles represent the two investigated sections in Guizhou (Yinjiang) and Hunan (Chuanyanping) Province, respectively. The blue triangles represent Ni–Mo–Se sulfide deposits. Black boxes represent barite deposits. (b) Generalized stratigraphy of the Chuanyanping section (Hunan Province) and the Yinjiang section (Guizhou Province). (For interpretation of the references to color in this figure legend, the reader is referred to the web version of the article.)

2008) were repeated before the determination of the unknown samples and indicated that the total analytical precision was better than ±0.1‰ (2σ). All results of the silicon isotopic analyses are reported as δ^{30}Si values against NBS-28 reference material as given in the delta notation: $\delta^{30}\mathrm{Si} = [(R_{\mathrm{sam}}/R_{\mathrm{std}}) - 1] \times 1000$, where R_{sam} and R_{std} are the ^{30}Si/^{28}Si ratios of the sample and NBS-28, respectively.

4. Results

Four stratigraphic intervals were delineated in the investigated chert samples which were largely based on observed Si isotopic variations, and also on Al_2O_3 content and field observations, with collections made from the two stratigraphic sections crossing the E–C boundary (Fig. 3). All the δ^{30}Si

Table 1
The silicon isotope composition, major and trace element data of cherts and other samples at the Ediacaran–Cambrian boundary in South China. YJ01–YJ11 were collected from Yinjiang section (Guizhou). CYP01–CYP13 were collected from Chuanyanping section (Hunan Province). I interval represents cherts from Liuchapo Formation within the Yinjiang section (YJ01–YJ09), II interval includes basal Cambrian chert from the Chuanyanping section (CYP02 and CYP03) and the Yinjiang section (YJ11), III interval represents middle cherts in Niutitang Formation of Chuanyanping section (CYP04–CYP08), and IV interval represents upper cherts of Chuanyanping section (CYP09–CYP11).

Interval	Sample no.	Description	$\delta^{30}Si$ (‰)	SiO_2 (%)	Al_2O_3 (%)	TiO_2 (%)	V (ppm)	Cr (ppm)	Ni (ppm)	Zn (ppm)	Sr (ppm)	Mo (ppm)	Sb (ppm)	Ba (ppm)	Rb (ppm)	Pb (ppm)	Th (ppm)
	CYP13	Black shale	1.0	61.25	4.89	0.21	263	37.2	102	175	87.6	116.67	2.78	664	44.3	41.5	4.5
	CYP12	Black shale	1.0	67.42	5.79	0.24	336	41.6	102	156	55.9	189.32	3.67	778	54.3	48.1	5.6
	CYP11	Bedded chert	1.1	95.89	1.28	0.06	11.6	14	7.38	23.1	10.7	1.61	1.18	464	7.5	3.9	2.2
IV	CYP10	Bedded chert	1.0	95.76	1.02	0.05	11.3	14.3	8.43	23.4	11.5	2.19	4.01	366	5.5	3.3	0.7
	CYP09	Bedded chert	1.2	96.5	1.16	0.05	11	11.2	5.45	24.9	21.6	3.04	1.15	1690	5.3	4.0	0.7
	CYP08	Bedded chert	0.4	97.1	0.46	0.01	15.2	11	7.57	42.6	7.78	1.25	0.76	206	2.3	0.1	5.3
	CYP07	Bedded chert	0.7	94.99	1.44	0.03	52.6	23.1	3.46	18.9	42.5	1.3	1.29	5750	8.8	2.3	0.8
III	CYP06	Bedded chert	0.5	95.02	1.01	0.03	25	16.2	4.34	18.6	19.9	7.47	6.39	2400	5.3	2.3	0.6
	CYP05	Bedded chert	0.2	96.28	0.89	0.02	19.1	14.8	6.82	8.91	34.3	1.65	0.85	2750	4.5	0.2	0.5
	CYP04	Bedded chert	0.1	93.07	1.45	0.04	28	18.3	5.01	14.4	120	3.69	1.41	9950	9.4	6.0	0.9
	CYP03	Bedded chert	−0.3	90.92	2.04	0.08	53.4	28.9	7.15	15.3	52.3	8.9	2.25	4480	15.1	15.5	1.3
	CYP02	Bedded chert	−0.5	85	3.91	0.14	72.6	34.3	6.99	27.7	84.3	7.59	3.24	6830	29.7	9.8	2.6
II	CYP01	K-bentonite	0.0	61.71	11.86	0.63	111	372	13.5	42.4	88.6	4.62	11.11	20,200	98.9	88.6	16.7
	YJ11	Bedded chert	−0.4	93.45	2.24	0.05	521	84	28	203	19.5	21	44.4	1210	21.5	3.2	1.2
	YJ10	K-bentonite	0.1	52.5	26.88	0.27	68	6	5.2	13	12.5	3.86	12.05	10,000	137.5	37.2	12.3
	YJ09	Bedded chert	0.4	97.56	0.42	0.04	119	39	22.6	85	11.5	4.09	6.49	280	4.1	3.1	0.5
	YJ08	Bedded chert	0.2	92.5	2.94	0.11	84	43	4.2	<2	26.2	1.26	24.7	1050	17.3	4.6	2.4
	YJ07	Bedded chert	0.6	94.39	2.29	0.1	127	56	20.8	6	11.6	1.42	3.61	1430	20.3	4.3	2.1
	YJ06	Bedded chert	0.5	89.5	4.91	0.16	34	25	12.3	42	39.8	0.76	3.56	1810	23.7	9.9	3.0
I	YJ05	Bedded chert	0.7	95.52	1.92	0.06	12	14	6.9	2	13.9	0.61	1.82	1640	8.4	5.9	1.2
	YJ04	Bedded chert	0.5	93.37	3.02	0.11	14	16	4	2	26.1	0.32	1.36	1880	5.1	4.4	1.7
	YJ03	Bedded chert	0.3	85.54	6.93	0.27	51	46	13.7	14	38.7	0.73	8.64	4540	42.5	6.2	4.0
	YJ02	Bedded chert	0.3	87.59	6.03	0.2	40	27	6.3	13	37.3	0.67	13.6	1950	28.6	7.2	2.6
	YJ01	Bedded chert	0.5	81.25	9.44	0.36	74	47	6.3	79	45.1	0.59	6.95	3130	57.2	5.6	5.2

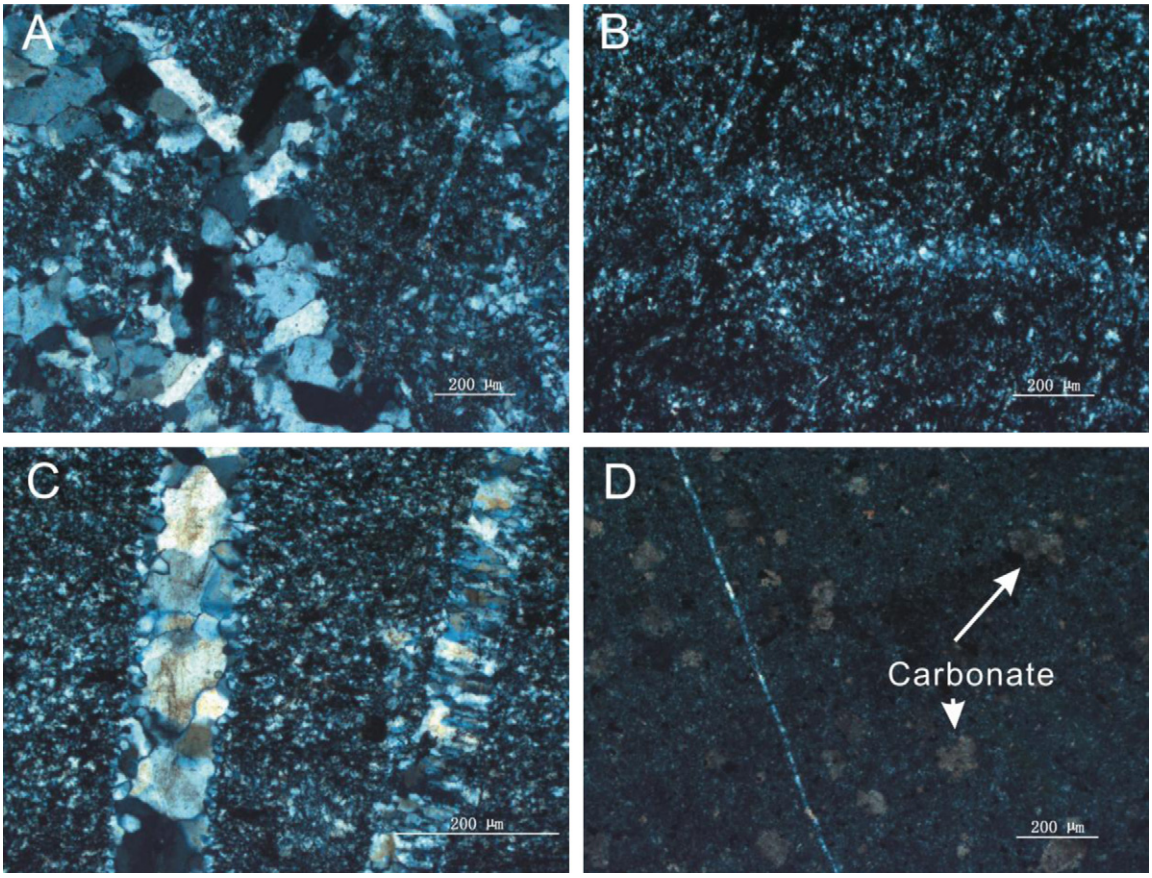

Fig. 2. Photomicrographs of chert samples: (A) geopetal structure containing micro-crystalline quartz, meso-crystalline quartz and mega-crystalline quartz. Crossed polars; bar scale – 200 μm. (B) Close-up of mesocrystalline quartz, showing the characteristic irregular crystal boundaries. Crossed polars; bar scale – 200 μm. (C) Numerous pseudo-parallel mega-crystalline quartz veins. Crossed polars; bar scale – 500 μm. (D) Photograph of carbonate. Crossed polars; bar scale – 200 μm.

values, and major and trace elemental data are presented in Tables 1–3.

4.1. Bedded cherts

The first interval chert samples with thin-layer structure show large Si isotopic variations, as much as 0.2–0.7‰ (Fig. 3). These chert samples are characterized by higher Al_2O_3 (1.92–9.44%, except YJ09) and TiO_2 (0.10–0.36%, except YJ05 and YJ09), which correlate negatively with SiO_2. They also show moderate enrichments in Ba (1050–4540 ppm, except YJ09), Cr (14.00–56.00 ppm), Ni (4.00–22.60 ppm), Sb (1.36–24.70 ppm), V (12.00–127.00 ppm), and Mo (0.30–4.09 ppm) compared to the average shale. The total REE + Y contents cover a wide range from 22.30 to 99.90 ppm. Most of these cherts often yield positive Eu anomalies (1.13–3.66), negative Ce anomalies (0.48–0.70) (Fig. 4a) and heterogeneous Y/Ho (27.08–36.25) (Table 2).

The second interval chert samples, locating on the K-bentonite layer, yield homogeneous $\delta^{30}Si$ value in the narrow range from −0.3‰ to −0.5‰ (Fig. 3). These cherts contain higher Cr, Mo, Ba, Zn, Rb and Sr than the average shale (Turekian and Wedepohl, 1961) and Franciscan cherts (Yamamoto, 1987). The total REE + Y contents cover a narrow range from 25.16 to 32.87 ppm. These cherts have obvious positive Eu anomalies at 5.32–9.89. The REE + Y patterns of the second interval cherts can be characterized by the enrichment of HREE compared to LREE and MREE ($0.44 < Pr_{SN}/Yb_{SN} < 0.70$) (Fig. 4b). Y/Ho ratios range from 25.58 to 36.19, representing chondritic (Y/Ho = 26–27, Pack et al., 2007) to slightly super-chondritic values.

The third and fourth interval cherts were firstly measured for Si isotope in this study. The $\delta^{30}Si$ values of the third interval cherts (0.1–0.7‰) are consistent with those of the first interval cherts. There is an increasing trend to heavier Si isotopic compositions in the Chuanyanping section (Fig. 3). Subsequently, the $\delta^{30}Si$ value achieves a peak of 1.2‰ in the fourth interval (contain more carbonate than III interval, Fig. 2D), which is similar to that of modern chemical sedimentary rocks (De La Rocha et al., 1997). The two interval cherts contain lower Al_2O_3 (0.46–1.45%) and TiO_2 (0.01–0.06%) than that of underlying strata. These chert samples are characterized by relative enrichment of LREE ($0.21 < Pr_{SN}/Yb_{SN} < 0.97$), chondritic to slightly super-chondritic Y/Ho ratios (25.43–30.95) and positive Eu anomalies (2.05–21.87) (Fig. 4c and d). The apparent difference in geochemical characteristics in the two interval chert samples was reflected by more carbonates and lower Cr, Mo, Ba, Sr content in the fourth interval (Table 1).

4.2. K-bentonite (an altered volcanic ash layer)

The $\delta^{30}Si$ value of the K-bentonites is close to modern felsic rocks (−0.1‰, Ding et al., 1996; −0.12‰, André et al., 2006). The K-bentonites from both sections, located between the first interval and second interval cherts, contain higher Al_2O_3 (11.86–26.88%) and TiO_2 (0.27–0.63%). They also show relatively high enrichments for Ba (up to 2.02%), Cr (up to 372 ppm), Zr (155.50–243.00 ppm), Mo (3.86–4.62 ppm) and Se (4.00–4.46 ppm). The REE + Y pattern of the two K-bentonites is slightly depleted LREE (Fig. 4b) and the samples have chondritic Y/Ho ratios (18.04–26.96).

Table 2
The rear earth element data of cherts and other samples at the Ediacaran–Cambrian boundary in South China.

Sample no.	La (ppm)	Ce (ppm)	Pr (ppm)	Nd (ppm)	Sm (ppm)	Eu (ppm)	Gd (ppm)	Tb (ppm)	Dy (ppm)	Y (ppm)	Ho (ppm)	Er (ppm)	Tm (ppm)	Yb (ppm)	Lu (ppm)	TREE (ppm)	Ce/Ce* (ppm)	Eu/Eu* (ppm)	Pr/Pr* (ppm)	Y/Ho (ppm)	$Pr/Yb_{(SN)}$ (ppm)
CYP13	15.6	29.9	3.18	12.5	2.5	0.57	2.58	0.41	2.43	18.3	0.57	1.65	0.23	1.47	0.21	92.09	0.91	0.99	1.02	32.39	0.85
CYP12	13.8	26.8	3	11.6	2.38	0.54	2.25	0.39	2.12	14.6	0.48	1.38	0.21	1.22	0.2	80.97	0.91	1.03	1.06	30.29	0.96
CYP11	1.97	2.47	0.31	1.03	0.18	0.11	0.21	0.04	0.3	2.66	0.09	0.29	0.05	0.34	0.05	10.1	0.66	2.41	1.21	30.3	0.36
CYP10	2.2	2.74	0.71	0.97	0.13	0.08	0.21	0.03	0.26	2.09	0.08	0.25	0.04	0.29	0.05	10.11	0.68	2.05	2.67	27.18	0.97
CYP09	2.15	2.89	0.35	1.15	0.18	0.29	0.19	0.04	0.28	2.3	0.08	0.26	0.04	0.29	0.05	10.54	0.7	6.81	1.2	28.15	0.47
CYP08	0.46	0.65	0.08	0.22	0.08	0.39	0.08	0.02	0.13	1.04	0.03	0.11	0.02	0.15	0.03	3.48	0.75	21.87	1.29	30.95	0.21
CYP07	2.99	3.77	0.52	1.6	0.19	0.89	0.35	0.04	0.3	2.33	0.08	0.27	0.05	0.32	0.06	13.75	0.66	15.18	1.3	28.04	0.63
CYP06	2.16	2.66	0.32	0.98	0.19	0.41	0.18	0.04	0.26	2.01	0.07	0.23	0.04	0.26	0.04	9.86	0.66	9.77	1.23	30.59	0.48
CYP05	1.53	2.08	0.28	0.84	0.17	0.48	0.19	0.03	0.26	1.79	0.07	0.21	0.04	0.26	0.04	8.28	0.71	11.49	1.33	25.64	0.44
CYP04	4.81	5.53	0.81	2	0.26	1.64	0.37	0.05	0.3	2.51	0.1	0.34	0.05	0.38	0.07	19.21	0.63	23.5	1.5	25.43	0.84
CYP03	5.89	7.69	1.09	3.25	0.33	0.78	0.4	0.07	0.47	3.78	0.13	0.48	0.09	0.61	0.1	25.16	0.68	9.43	1.35	29.08	0.7
CYP02	7.89	9.68	1.22	3.61	0.51	1.1	0.47	0.1	0.76	5.55	0.22	0.65	0.11	0.87	0.13	32.87	0.66	9.89	1.28	25.58	0.55
CYP01	59.9	56.5	8.03	19.3	1.37	3.28	2.3	0.42	3.29	25.6	0.95	3.18	0.54	4.18	0.65	189.48	0.54	8.11	1.5	26.98	0.75
YJ11	4.1	6.45	0.9	3.6	0.87	1.18	1.09	0.17	1.01	7.6	0.21	0.65	0.1	0.8	0.13	28.86	0.73	5.32	1.15	36.19	0.44
YJ10	5.5	15.55	2.66	11.8	3.52	2.48	2.96	0.6	4.2	17.5	0.97	3.01	0.5	3.51	0.57	75.33	0.91	3.37	1.18	18.04	0.3
YJ09	3.5	3.94	0.92	4	0.83	0.08	0.83	0.17	0.83	5.8	0.16	0.55	0.08	0.52	0.09	22.3	0.48	0.42	1.33	36.25	0.69
YJ08	7.9	11.55	1.96	7.9	1.67	0.4	1.33	0.3	1.02	6.5	0.24	0.82	0.13	0.76	0.13	42.61	0.65	1.18	1.25	27.08	1.01
YJ07	8.4	11.3	2.2	9.4	2.04	0.69	2.16	0.41	2.45	14	0.47	1.45	0.23	1.62	0.23	57.05	0.57	1.44	1.27	29.79	0.53
YJ06	10.9	17.3	2.69	11.1	2.35	0.44	1.61	0.23	1.37	8.7	0.29	0.91	0.14	0.97	0.16	59.16	0.7	0.99	1.19	30	1.09
YJ05	5.7	7.75	1.2	4.1	0.69	0.32	0.62	0.08	0.52	3.8	0.12	0.4	0.06	0.45	0.08	25.89	0.66	2.15	1.32	31.67	1.05
YJ04	6	7.37	1.06	3.7	0.58	0.43	0.46	0.07	0.48	3.4	0.11	0.41	0.07	0.52	0.09	24.75	0.62	3.66	1.26	30.91	0.8
YJ03	16.7	21.9	3.36	12.1	2.01	1.35	1.61	0.28	1.89	14	0.44	1.38	0.22	1.65	0.3	79.19	0.64	3.29	1.28	31.82	0.8
YJ02	14.6	17.9	2.83	10.3	1.66	0.41	1.52	0.26	1.74	13	0.4	1.24	0.2	1.43	0.23	67.72	0.6	1.13	1.29	32.5	0.78
YJ01	29.6	32	4.62	14.4	1.69	0.72	1.49	0.21	1.36	10.4	0.32	1.15	0.2	1.47	0.27	99.9	0.58	1.99	1.34	32.5	1.23

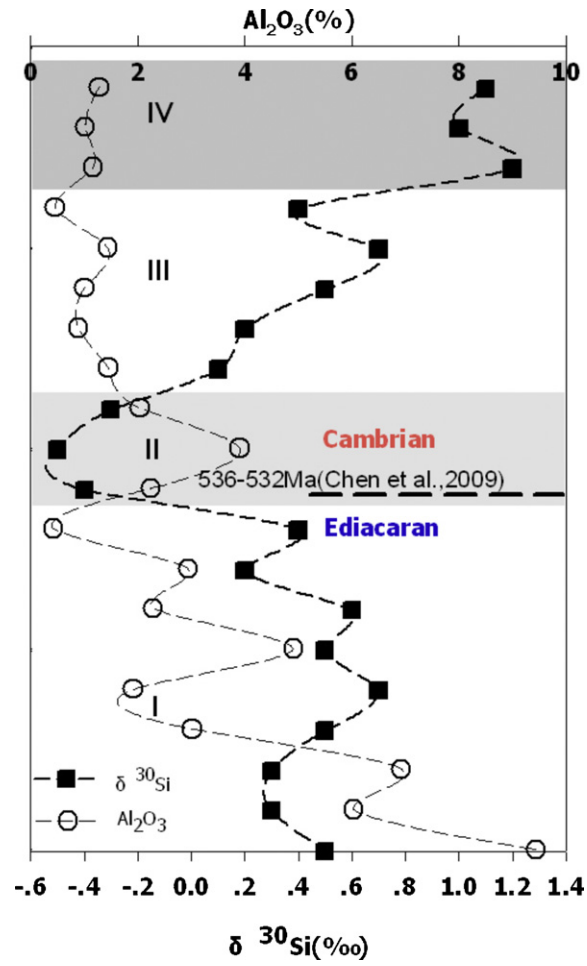

Fig. 3. Silicon isotope and Al_2O_3 concentration curves of cherts of Ediacaran–Cambrian boundary transition from the Chuanyanping section (Hunan Province) and the Yinjiang section (Guizhou Province).

4.3. Black shale

The $\delta^{30}Si$ value of black shales on the top of the fourth interval cherts is 1.0‰, similar to that of the fourth interval chert samples. However, these black shales contain less Ba (664.00–778.00 ppm), and abundant Cr (37.20–41.60 ppm), Zn (156.00–175.00 ppm), and V (263.00–336.00 ppm). The total REE+Y content is higher (80.97–92.09 ppm) than most chert samples. The REE+Y pattern is flat, lacking positive Eu anomalies (Fig. 4d). Their Y/Ho ratios (30.29–32.39) are different from those of normal marine sediments (60). Some framboidal pyrite is present in these black shales indicating anoxic conditions.

5. Discussion

5.1. Trace element evidence for the origin of cherts at the E–C transition

5.1.1. REE geochemistry

It is necessary to estimate the influence of terrigenous materials before interpreting the REE signatures of the studied chert samples because they formed in a marginal zone. No systematic relationships of Pr/Yb_{PAAS}, Y/Ho, Ce/Ce* and Eu/Eu* with TiO_2 were observed, which suggested that the REE characteristics of the cherts are not significantly contaminated by terrigenous materials, although there is a positive relationship between total REE and TiO_2 contents (Sugahara et al., 2010).

Table 3
TiO_2-normalized values of trace elements for cherts and K-bentonite in this study, Franciscan cherts within 5 m from the basal basalt (Yamamoto, 1987) and average shale (Turekian and Wedepohl, 1961).

Sample no.	Cr/TiO_2	Ni/TiO_2	Zn/TiO_2	Rb/TiO_2	Sr/TiO_2	Zr/TiO_2	Mo/TiO_2	Ba/TiO_2	Pb/TiO_2	Th/TiO_2
CYP11	233	123	385	125	178	205	27	7733	65	37
CYP10	286	169	468	110	230	206	44	7320	65	14
CYP09	224	109	498	105	432	208	61	33,800	80	14
CYP08	1100	757	4260	230	778	646	125	20,600	12	530
CYP07	770	115	630	292	1417	430	43	191,667	78	25
CYP06	540	145	620	177	663	370	249	80,000	77	20
CYP05	740	341	446	223	1715	520	83	137,500	11	23
CYP04	458	125	360	236	3000	380	92	248,750	150	22
CYP03	361	89	191	189	654	321	111	56,000	194	16
CYP02	245	50	198	212	602	310	54	48,786	70	19
CYP01	590	21	67	157	141	386	7	32,063	141	27
YJ11	1680	560	4060	430	390	300	420	24,200	64	24
YJ10	22	19	48	509	46	576	14	37,037	138	46
YJ09	975	565	2125	103	288	220	102	7000	78	13
YJ08	391	38	–	157	238	273	11	9545	42	22
YJ07	560	208	60	203	116	248	14	14,300	43	21
YJ06	156	77	263	148	249	201	5	11,313	62	19
YJ05	233	115	33	140	232	250	10	27,333	98	20
YJ04	145	36	18	46	237	215	3	17,091	40	15
YJ03	170	51	52	157	143	213	3	16,815	23	15
YJ02	135	32	65	143	187	193	3	9750	36	13
YJ01	131	18	219	159	125	174	2	8694	16	14
Franciscan chert	360	440	2100	43	350	340	48	5600	450	33
Average shale	120	88	120	180	390	210	3	750	26	15

Recently, Chang et al. (2008) suggested that cherts from Liuchapo Formation were chemically precipitated from seawater based on rare earth element patterns, positive La anomalies, minor positive Eu and higher Y/Ho (33.6–43.9). Their samples should be included in the first interval cherts in this study. However, variable positive Eu anomalies (0.42–3.66) and variable Y/Ho (27.08–36.25) were observed in our chert samples which suggested that there maybe another source of Eu apart from seawater. At an earlier time, Sverjensky (1984) reported that the enrichment of Eu was only observed under extremely reducing and alkaline conditions, but this has not been reported in nature (Steiner et al., 2001). Moreover, the redox condition of this study area is an anoxic environment with Fe enrichment, rather than an extremely H_2S-rich euxic environment (Chang et al., 2010). Mobilization of Eu has been

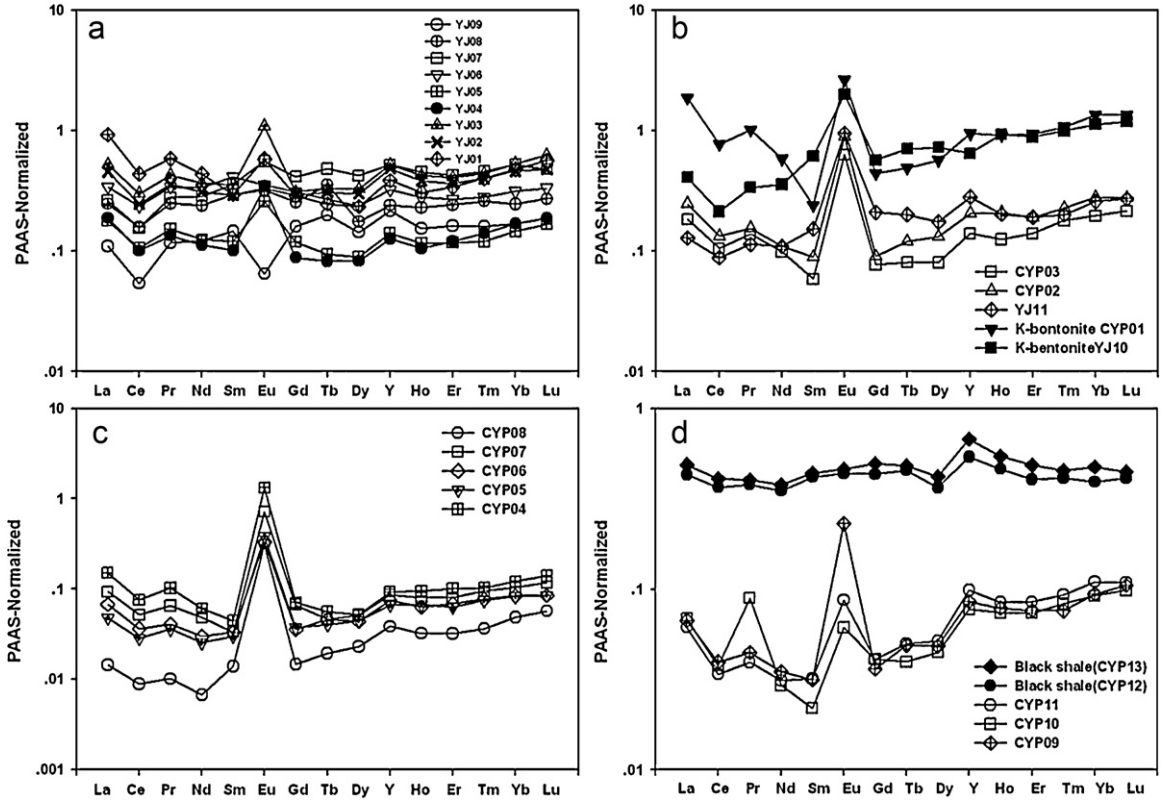

Fig. 4. Shale-normalized (PAAS; Post-Archean Australian Shale) REE + Y patterns of different samples from the investigated Chuanyanping section (Hunan Province) and the Yinjiang section (Guizhou Province): (a) I interval chert; (b) II interval chert and K-bentonite; (c) III interval chert; (d) IV interval chert and upper black shale.

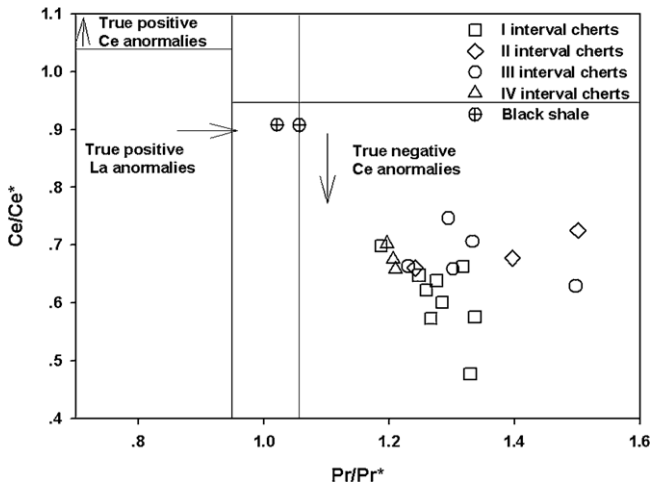

Fig. 5. Plot of Ce/Ce* and Pr/Pr* anomalies for our cherts and black shales. Positive La anomalies are only present in Cambrian Niutitang Formation black shales whereas all analyzed cherts show true negative Ce anomalies. We used approach first described by Bau and Dulski (1996) to discriminate between positive La and negative Ce anomalies.

found in recent hydrothermal seafloor systems at spreading zones and in the Red Sea (Michard et al., 1983), which indicates that Eu anomalies may be used to distinguish hydrothermal alterations. In Precambrian oceans, REE were not scavenged by Fe–Mn oxyhydroxides shortly after their emission from hydrothermal vent because of low levels of oxygen (Farquhar et al., 2000). The influence of hydrothermal fluid (Danielson et al., 1992) characterized with Eu-anomalies could be a signature of Precambrian ocean. In the studied area, however, phosphorite interbedded with chert show higher Y/Ho (up to 56) and negative Eu anomalies (Shields and Stille, 2001) which might suggest that the positive Eu anomaly is not a signature of the ambient shallow seawater. Bolhar et al. (2005) suggested that high temperature water–rock interaction could not fractionate Y and Ho resulting in the chondritic values of hydrothermal fluids (Y/Ho as 26–27). In the surface environment, fractionation of Y and Ho could be caused by the scavenging of REE by particulate matter in the water column (Nozaki et al., 1997). So the positive Eu anomalies and slightly super-chondritic Y/Ho in the first interval cherts provide evidence for the contribution of hydrothermal fluids.

The second, third and fourth interval cherts also show obvious positive Eu anomalies and slightly super-chondritic Y/Ho, which reflects the mixing of seawater with high temperature (>250 °C) hydrothermal fluids (Bolhar et al., 2004, 2005; Friend et al., 2008) (Fig. 4b–d). The strong Eu anomalies were also observed in the Ni sulfide minerals of Ni–Mo–PGE ore overlain on the fourth interval cherts (Steiner et al., 2001). The end of the hydrothermal activity is demonstrated by straight PAAS normalized REE patterns, positive La anomalies and abundant clastic materials in the upper black shales, which are representative of typical detrital shales (Fig. 4d).

Fig. 5 shows the relationship between Ce/Ce* and Pr/Pr* which indicates the presence of obviously negative Ce anomalies in all the chert samples. Ce anomalies as low as 0.48 demonstrated that the decoupling of redox sensitive Ce from its redox insensitive neighbors did occur in the depositional environment of all the cherts (Bau and Koschinsky, 2009). By contrast, the black shale did not contain the negative Ce anomalies that recorded the anoxic conditions of the ambient seawater.

5.1.2. Trace element geochemistry

Trace element concentration normalized by TiO_2 is a useful index in understanding the chemical signature and depositional environment of siliceous rocks (Sugisaki, 1984). We used TiO_2 normalized values to estimate the hydrothermal components in the studied cherts listed in Table 3. The first interval cherts have higher Cr, Mo, Ba and Pb values than that of the average TiO_2 normalized shale which suggested that the excess trace elements were not mainly derived from seawater. The third interval cherts are not only enriched in Cr, Mo and Ba, but also are enriched in Ni, Zn, Rb, Sr and Zr compared to the average shale. This observation for the third interval is similar to that of the Franciscan chert, which is interpreted as hydrothermal origin by Yamamoto (1987). The difference of elemental distribution between I and III interval could be explained by two alternative reasons: (1) mixing of volcanic materials (clastic materials) and seawater for I interval cherts and (2) mixing of hydrothermal fluids and seawater for III interval cherts. The obvious positive relationships of Cr/TiO_2, Ba/TiO_2 and SiO_2/TiO_2 indicated that most of Cr and Ba were derived from Si-rich hydrothermal fluids. In the modern ocean, higher Ba concentrations are interpreted as higher biomass and productivity in upper mixed layer (Jacquet et al., 2007). It is noted that all the cherts contain abundant Ba compared to the organic-rich black shales. This also verifies that higher Ba concentration in the studied cherts was not controlled by biomass.

5.2. Silicon isotopic system from the E–C boundary

The Si isotopic compositions of all the chert samples from the E–C boundary could be divided into three groups (Fig. 3): (1) the first and third interval cherts cover a wide range ($\delta^{30}Si$ = +0.2‰ to +0.7‰); (2) the second interval chert samples show the most negative values ($\delta^{30}Si$ = −0.3‰ to −0.5‰); (3) the fourth interval cherts yield the most positive $\delta^{30}Si$ values showing a much more restricted range (+1.1‰ to +1.2‰). Two mechanisms could be used to explain the Si isotopic variations in these samples. First, the variations could reflect the mixing of different sources of silicon with various isotopic compositions (Van den Boorn et al., 2007). Second, fractionation mechanisms during silicon deposition from silicon-bearing fluids could account for the variations (Georg et al., 2007; Beucher et al., 2008; Van den Boorn et al., 2010).

5.2.1. Mixing model

Only based on the silicon isotopic variation (as low as −0.5‰ and as high as +1.2‰) in these studied cherts, it is very difficult to distinguish if the result arose due to multiple sources of silicon, or Si isotopic fractionation during Si deposition. However, we found that the mineralogy of our cherts is similar to that of Archean cherts from Carbonne et al. (2011) and the highest $\delta^{30}Si$ value in this study is similar to that of Archean cherts from Van den Boorn et al. (2007, 2010) which maybe indicate that our cherts could precipitate from identical Si over saturated condition of reported on Archean cherts. So the mixing model established by Van den Boorn et al. (2007) was applied in our study. And the three end-members model for these cherts from E–C boundary: (1) hydrothermal fluids, (2) silicon-rich seawater and (3) volcanic materials, also can be recognized after combining Si isotopes with Al_2O_3, as illustrated in the $\delta^{30}Si$-Al_2O_3 diagram (Fig. 6). Most of the first interval chert samples fall on the Al_2O_3-rich side of the graph (>2.94%), whereas other chert samples are depleted in Al_2O_3 (<2.24%). The Al_2O_3-rich end-member reflects primarily volcanic materials as it has a $\delta^{30}Si$ value close to or slightly above 0‰. The Al_2O_3-poor cherts could then be interpreted as chemical precipitation from mixtures of ^{30}Si-rich and ^{30}Si-poor fluid (Van den Boorn et al., 2007, 2010).

Indeed, the highest $\delta^{30}Si$ value (1.2‰) is similar to that of the Cambrian Storm cherts from New York State (the most positive value is 1.3 ± 0.3‰, Robert and Chaussidon, 2006), and that of stratiform cherts from the North Pole (the most positive value is 1.3‰, Van den Boorn et al., 2010). The fourth interval cherts also

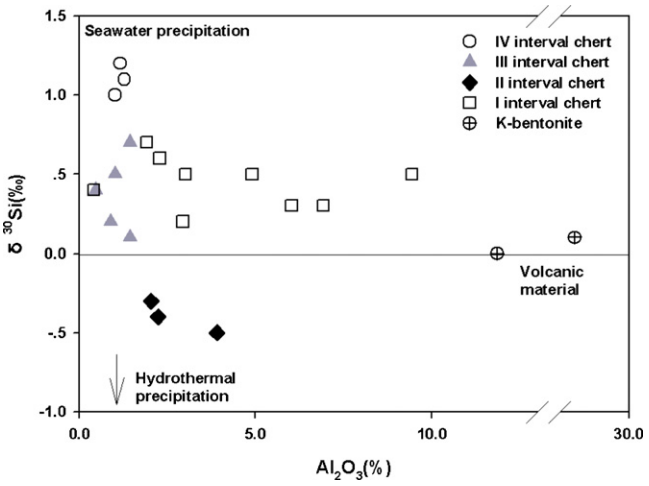

Fig. 6. Correlation between Al_2O_3 content and $\delta^{30}Si$ value of chert and K-bentonite samples.

show the lowest Al_2O_3, TREE and Ba content, similar to seawater REE pattern. All these observation could have been interpreted as the influence of ^{30}Si-rich seawater. It also may indicate that Cambrian seawater had a positive $\delta^{30}Si$ value greater than 1.2‰, because of the large fractionation factor between fluid and precipitate Si (−1.5‰). The activity of diatoms and sponges preferentially removes ^{28}Si from modern seawater, while the continuous supply ^{30}Si of river led to the strong positive $\delta^{30}Si$ of modern seawater (De La Rocha et al., 1997; De La Rocha, 2003). However, Siever (1992) pointed out that there is a lack of an efficient bio-mediated removal mechanism in Precambrian ocean, which resulted in silicon saturation in seawater. The Precambrian silicon cycle was dominated by inorganic reactions, which further enrich the remaining seawater with heavier Si isotopes (such as adsorption of silicon in Fe oxide, Delstanche et al., 2009, or chemical precipitation of silicon, Van den Boorn et al., 2010; Abraham et al., 2011).

The lowest $\delta^{30}Si$ group (−0.5‰ to −0.3‰) in our samples resemble the $\delta^{30}Si$ values of hot springs in Yellowstone National Park, Wyoming and Mammoth, California (USA) (Douthitt, 1982), and those of black siliceous precipitates forming at temperatures above 100 °C (−0.6‰ to −0.4‰, Coplen et al., 2002), which may indicated a significant influence of hydrothermal fluids, combined with obviously Eu anomalies, highly Ba level and unusual correlation between Ce/Ce* and Pr*Pr* (Fig. 5). The silicon concentration of hydrothermal fluids is controlled by equilibration between quartz and fluid at high temperature (200–400 °C) and pressure (100–500 bars) in the reaction zone of convection cells (Von Damm et al., 1991). As hydrothermal fluid approaches to the near surface environment, the sudden drop of temperature and pressure results in over-saturation with respect to silicon in the hydrothermal fluid. It is true that the $\delta^{30}Si$ value of cherts should be lower than the initial Si isotopic composition of hydrothermal fluids (<−0.3‰, Abraham et al., 2011). However, the $\delta^{30}Si$ value of the second group cherts is similar to that of Bulk Silicate Earth (BSE) and hydrothermal fluids, which may suggest that the mixing of seawater with the hydrothermal fluid took place before the chemical precipitation of silicon.

Medium $\delta^{30}Si$ values of the first and third interval cherts are similar to the positive values of pure chemical precipitation cherts (Van den Boorn et al., 2010). And the first interval cherts was interpreted as hydrothermal precipitation by Peng et al. (1999). From the mixing model, the first interval cherts show a mixture of seawater and volcanic materials, which also can be confirmed by the real negative Ce/Ce*, higher TREE, Al_2O_3 and TiO_2 level. On the other hand, the third interval cherts show a mixture of seawater and hydrothermal fluids, which is consist with the observation of the highly Eu/Eu*, higher Ni and Zn content, lower TREE, Al_2O_3, TiO_2 level, abnormal relationship of Ce/Ce* and Pr/Pr* (Fig. 5). However another alternative deduction was not excluded based on the depositional setting of the sedimentary succession of these two chert intervals (Fig. 1B). The higher Al_2O_3 in the first interval cherts also could be derived from the basal black shale, enriched in TiO_2, Al_2O_3 and total REE content.

In addition, the first and third interval cherts contain micro- and meso-quartz grains and quartz veins with mega-crystalline quartz (Fig. 2C), similar to that of cherts from the Onverwacht Group (Carbonne et al., 2011). No obvious differences in silicon isotopic composition between microquartz grains and quartz veins were observed in Archean cherts, which suggested that fluid circulation did not largely affect the $\delta^{30}Si$ value of the microquartz grains (Carbonne et al., 2011). Although we lack a $\delta^{30}Si$ value of the microquartz grains and quartz veins in this study, we maintain that the silicon isotopic composition in these two chert intervals is the primary isotope signature. It is true that the $\delta^{30}Si$ value of Cambrian quartz veins is higher than Archean quartz veins, which is consistent with the suggestion of lighter silicon precipitation initially from the dissolved phase during evolution of hydrothermal fluids from 3500 Ma to 800 Ma (Robert and Chaussidon, 2006). Further work on the quartz veins should be undertaken to examine this speculation.

5.2.2. Fractionation model

Si isotope fractionation mechanisms can be better explained by two separate trends (one linear and one exponential, as shown in Fig. 7) as opposed to one general linear trend. Fig. 7 shows the predicted $\delta^{30}Si$ evolution of fluid and co-existing deposits during closed-system (steady-state) and open-system (Rayleigh-type kinetics) fractionation, respectively, based on the following equations (Georg et al., 2007):

$$\text{Steady sate system}: \quad \delta^{30}Si_{\text{dissoved}} = \delta^{30}Si_{\text{initial}} - \varepsilon * (1-f);$$
$$\delta^{30}Si_{\text{deposit}} = \delta^{30}Si_{\text{initial}} + \varepsilon * f$$

$$\text{Rayleigh type system}: \quad \delta^{30}Si_{\text{dissoved}} = \delta^{30}Si_{\text{initial}} + \varepsilon * \ln(f);$$
$$\delta^{30}Si_{\text{deposit}} = \delta^{30}Si_{\text{dissoved}} + \varepsilon$$

where $\delta^{30}Si_{\text{dissoved}}$ is the Si isotope composition of remaining fluids, $\delta^{30}Si_{\text{deposit}}$ is the Si isotope composition of chert samples; $\delta^{30}Si_{\text{initial}}$ is the initial silicon isotope composition which we set to be the Bluk Silicate Earth of −0.3‰ (Fitoussi et al., 2009; Savage et al., 2010) and f is the fraction of Si remaining in the initial fluids. ε is the difference between $\delta^{30}Si$ of dissolved silicon and precipitated silicon. The isotopic fractionation between dissolved and precipitated silicon has not been determined for cherts. We therefore adopt two different estimates for the fractionation factor ε: one small value is −1.0‰, based on the difference between experimentally precipitated silicon and dissolved silicon (De La Rocha et al., 1997; Ding et al., 1996, 2004) and another large value −2.3‰, based on the difference between the most negative $\delta^{30}Si$ of chert measured in the Pilbara Craton and hydrothermal fluids (Van den Boorn et al., 2010).

According to Fig. 7, only Rayleigh-type fractionation could achieve the more positive ^{30}Si value for cherts after losing enough precipitated silicon. For $\varepsilon = -2.3$‰, the removal of 81% of original dissolved silicon from solution results in as high as 1.2‰ (our most positive ^{30}Si value found in the fourth interval cherts). Also, the most positive ^{30}Si value can be generated by Rayleigh fractionation after precipitation of 92% silicon for $\varepsilon = -1.0$‰. In a Rayleigh model, a gradual increase of $\delta^{30}Si$ in solution, accompanying with the

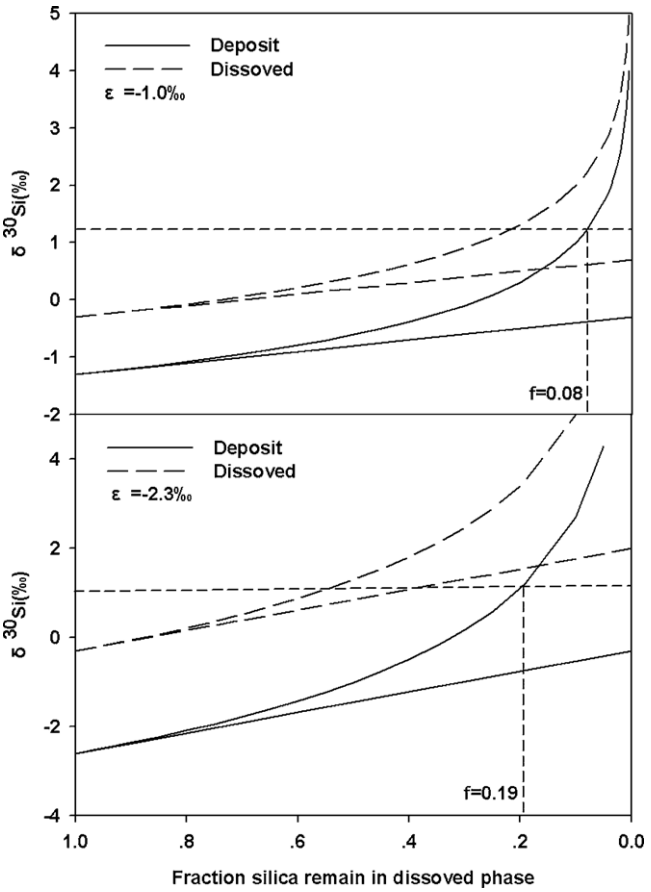

Fig. 7. Si isotope fractionation during precipitation from dissolved phase, modeled as closed-system (steady-state) and open-system (Rayleigh-type kinetics) fractionation for $\varepsilon = -1.52‰$ and $-3.0‰$. The vertical short dash lines represent f at which $\delta^{30}Si_{deposit}$ of 1.2‰ (based on Van den Boorn et al., 2010).

decreasing of silicon concentration of fluid, was observed (Li et al., 1995; Ziegler et al., 2005). Therefore, the fraction of higher $\delta^{30}Si$ that precipitates is much smaller than the earlier precipitates (Heck et al., 2011). Recently, Robert and Chaussidon (2006) suggested that silicon precipitation from hydrothermal fluids depends on the difference between the temperature and pressure conditions, and that the silicon content of hydrothermal fluids can be estimated from a fixed seawater temperature and the estimated f. Their model was also used by Van den Boorn et al. (2010) who estimated that the silicon concentration in Archean hydrothermal fluids was high enough to produce chert with a positive $\delta^{30}Si = 1.3‰$ near a vent. They also pointed out that the silicon concentration in the hydrothermal fluid would largely overlap the P–T range of present-day hydrothermal systems when the seawater temperature was assumed as 55 °C. In this study, the estimated maximum silicon concentration in E–C hydrothermal fluids would be greater than that of Archean, as speculated by Van den Boorn et al. (2010), even though a lower seawater temperature (25 °C) was used to calculate silicon concentration for the higher ε value ($-1.0‰$). This deduction would argue against the conclusion that abundant dissolved silicon in hydrothermal fluid precipitated from 3500 Ma to 800 Ma (Robert and Chaussidon, 2006). The contradiction could be attributed to overestimating the fractionation factor ($-1.0‰$) and underestimating the initial $\delta^{30}Si$ value ($-0.3‰$).

The average silicon isotope fractionation in the ocean would have been closer to the value ($-3.8‰$) of sponges before the onset of the diatom-dominated ocean (De La Rocha, 2003; De La Rocha and Bickle, 2005). During the transition from a pre-diatom ocean to a diatom-dominated ocean, the average $\delta^{30}Si$ value of seawater would drop from the higher value of 1.9‰ down to roughly 0.8‰ in the modern ocean (De La Rocha and Bickle, 2005). At the same time, the silicon concentration maintained strongly oversaturated conditions during the Precambrian transitioning to under-saturated status after the Cenozoic. We predict that the $\delta^{30}Si$ values of seawater at E–C boundary should vary from +3.5‰ to +2.2‰ based on the different ε ($-2.3‰ < \varepsilon < -1.0‰$) (Fig. 7). The deduction is consistent with the $\delta^{30}Si$ value of silicified stromatolite ($\delta^{30}Si = +2.4‰$ to +3.4‰, Ding et al., 1996) and that of cherts (most of +2.14‰ to +3.48‰, Robert and Chaussidon, 2006) from the Jixian Group in North China during the Mesoproterozoic, which may reflect the silicon isotopic composition of Mesoproterozoic seawater.

5.3. The volcanic activity during Ediacaran–Cambrian transition

In both investigated sections, an altered volcanic ash layer of K-bentonite was found associated with the E–C transitional interval (Fig. 1b). The $\delta^{30}Si$ values of the two K-bentonites were in a narrow range from 0.0‰ to +0.1‰ which is similar to the result of Li et al. (1995), who found that the $\delta^{30}Si$ value of the fifth stratum volcanic ash in the Meishucun profile of Yunna Province was 0.0‰ to +0.1‰. Abraham et al. (2011) suggested that the $\delta^{30}Si$ value of unsilicified basalts is similar to that of Bulk Silicate Earth ($\delta^{30}Si = -0.28‰$, Fitoussi et al., 2009). The $\delta^{30}Si$ value of altered basalts would increase during the silicification processes which could explain why the $\delta^{30}Si$ values of these K-bentonites are closer to zero.

It is interesting that atop the K-bentonite strata, an apparent negative Si isotopic excursion was observed in the second interval cherts (Fig. 3). The phenomenon was also observed in other stratigraphic sections in South China, such as the Meishucun section in Yunnan Province (Li et al., 1995), and the Sancha and the Taojiang sections in Hunan Province (Wang and Chen, 1996; Jiang and Li, 2005). Based on the $\delta^{30}Si$ value of this interval, they suggested that these cherts were formed by hydrothermal mineralization. The temperature of the mixed fluid formed from seawater and hydrothermal fluid was estimated as 80–98 °C on the basis of the relationship of O isotopes between cherts and seawater (Jiang and Li, 2005). Significant enrichment in trace metals such as V, Mo, Zn, As, and Ba also suggested that hydrothermal fluid played an important role in governing the geochemical characters of these cherts. The higher total REE content of the second interval cherts could be derived from volcanic materials. In fact, it is difficult to distinguish whether the apparent negative Si isotopic excursion was controlled by hydrothermal fluid or addition of volcanic materials, although previous study found that the oxygen isotopic composition of the second interval cherts ($\delta^{18}O = 18.12–22.55‰$) showed hydrothermal characteristics ($\delta^{18}O = 20.7–23.0‰$), rather than that of volcanic genesis cherts ($\delta^{18}O = 1.9–9.2‰$) and normal marine cherts ($\delta^{18}O = 25.6‰$) (Jiang and Li, 2005). We are inclined to believe that volcanic activity could trigger a more intense hydrothermal fluid flux with higher temperature and lower $\delta^{30}Si$ into the ocean.

More than a dozen volcanic ash beds are documented from several horizons of the E–C transition of the Yangtze Platform (Zhang et al., 2004; Zhou et al., 2008). Preserved bed thicknesses range from several millimeters to several centimeters. These volcanic ash deposits were separated into two types. The first type consists of tuffites that were deposited at considerable distance from the volcanic center (Zhang et al., 2004). The second type has been altered to K-bentonites, which are soft, generally thinly bedded (from several mm to 10 cm) (Luo et al., 2005). From field observation and previous study, we maintain that the K-bentonites are the product of alteration of volcanic ash that has fallen into the oceans. Thus, the

K-bentonites may represent a relatively active tectonic background and may also suggest changes in the marine sedimentary environment. These K-bentonites are not only distributed on the Yangtze Platform, but also on other sites in the world, such as Oman of the Arabian Penninsula (Amthor et al., 2003). Thus, these ash layers and the second interval cherts could be taken as markers for volcanic eruption events and used for stratigraphic correlation.

5.4. Hydrothermal condition of Ediacaran–Cambrian boundary

The temperature of the hydrothermal fluids present at E–C boundary were inferred from the homogenization temperature of fluid inclusions within quartz that crosscut the Ni–Mo–PGE polymetallic ore deposit hosted in black shale overlying the fourth interval cherts (260 °C, Lott and Coveney, 1996), and of fluid inclusions within the barite deposit from Guizhou Province (150–190 °C, Yang et al., 2008). These authors also suggested that the hydrothermal fluids could have higher temperature and lower salinities (<10% NaCl) before mixing with seawater and phase-separation occurred. In this study, the wide range of δ^{30}Si, highly positive Eu anomalies, unusual correlation between Ce/Ce* and Pr/Pr*, and highly Cr, Mo, Ba, Ni, Zn-rich observed in these cherts of this study also indicated occurrence of high temperature hydrothermal fluids.

Given that hydrothermal venting took place both along the northern and southern marginal zones of Yangtze Platform with a lateral extent of about 20–50 km, Chen et al. (2009) estimated the area of the vent fields at 50,000–120,000 km^2. The estimate provides reasonable evidence as to why bedded chert deposits so dominate off the platform interior of Yangtze Platform in South China. These could not be deposited in a normal continental marginal slope to basin environment, rather they were likely precipitated in the marine systems upon the rapid mixing of upwelling hydrothermal silicon-rich fluids with the cool seawater (Herzig et al., 1988; Stüben et al., 1994). In the context of the accelerated breakup of the Rodinia super-continent in Late Neoproterozoic (Veevers et al., 1997), the South China block was initially subjected to rifting (Zheng et al., 2008), then evolved into a passive continental margin basin under extensional tectonics (Wang and Li, 2003), resulting in episodic thermal anomalies and faulting reactivation of the antecedent amalgamation zone. Under these circumstances, hydrothermal fluids enriched in ^{28}Si and other metals at the deep-seated heat source were driven upwards along fault conduits, and finally vented into the ocean, forming hydrothermal silica chimneys or bedded chert deposits, even polymetallic sulfide deposits.

In summary, the hydrothermal activities across the E–C transition could be an alternative candidate to explain the vast changes in the oceanic environment, the occurrence of bedded cherts and massive metallic ore deposits and the biological diversity during the E–C transition.

6. Conclusions

Silicon isotopic composition and other traditional geochemical characteristics were measured to unlock the information recorded in cherts from the Ediacaran–Cambrian transition in the Yangtze Platform. Slightly positive δ^{30}Si values (+0.2‰ to +0.7‰) in the first and third interval cherts indicated that the initial precipitating solution is a mixture of light Si isotope-rich hydrothermal fluids and volcanic materials and heavy Si isotope-rich seawater, from which we proposed that chemical deposition occurred after the mixing of cool seawater with relatively hot hydrothermal fluids. The most negative δ^{30}Si values (−0.3‰ to −0.5‰) in the second interval cherts were interpreted as an increase in volcanic materials together with hydrothermal fluid. Silicon isotope fractionation model suggested that the most positive δ^{30}Si (+1.2‰) can be achieved by precipitation of Si from hydrothermal fluid. On the other hand, the obvious positive Y anomalies and negative Ce anomalies of these cherts also reflect the contribution of seawater. We incline to think that the highest δ^{30}Si should represent chemical precipitation from seawater, although the precipitation of enough silicon also can results in a δ^{30}Si of the remaining hydrothermal fluid near that of seawater. The hydrothermal activity across the Ediacaran–Cambrian transition was likely of global significance, which could be a candidate to trigger the anoxic oceanic environment, the occurrence of chert deposits and massive sedimentary ore deposits and the diversification of life.

Acknowledgments

The project was funded by the 12th Five-Year Plan project of State Key Laboratory of Ore-deposit Geochemistry, Chinese Academy of Sciences (SKLODG-ZY125-07), the Natural Science Foundation of China (40803016, 40930425) and the Ministry of Science and Technology of the PRC (KCZX20100104), MLR Public Benefit Research Foundation (201011027) and China Geological Survey Foundation (1212011121069). We thank Mr. Anhua Wang engineer for helping in field work, Pr. Yuzhou Qiu and Mr. Kyle Trostle for improving the manuscript.

References

Abraham, K., Hofmann, A., Foley, S.F., Cardinal, D., Harris, C., Barth, M.G., André, L., 2011. Coupled silicon–oxygen isotope fractionation traces Archean silicification. Earth and Planetary Science Letters 301, 222–230.

Amthor, J.E., Grotzinger, J.P., Schroder, S., et al., 2003. Extinction of Cloudina and Namacalathus at the Precambrian-Cambrian boundary in Oman. Geology 31, 431–434.

André, L., Cardinal, D., Alleman, L.Y., Moorbath, S., 2006. Silicon isotopes in 3.8 Ga West Greenland rocks as clues to the Eoarchaean supracrustal Si cycle. Earth and Planetary Science Letters 245, 162–173.

Bau, M., Dulski, P., 1996. Distribution of yttrium and rare-earth elements in the Penge and Kuruman iron-formations, Transvaal Supergroup, South Africa. Precambrian Research 79, 37–55.

Bau, M., Koschinsky, A., 2009. Oxidative scavenging of cerium on hydrous Fe oxide: evidence from the distribution of rare earth elements and yttrium between Fe oxides and Mn oxides in hydrogenetic ferromanganese crusts. Geochemical Journal 43, 37–47.

Beucher, C.P., Brzezinski, M.A., Jones, J.L., 2008. Sources and biological fractionation of silicon isotopes in the Eastern Equatorial Pacific. Geochimica et Cosmochimica Acta 72, 3063–3073.

Blake, R.E., Chang, S.J., Lepland, A., 2010. Phosphate oxygen isotopic evidence for a temperate and biologically active Archean ocean. Nature 464, 1029–1032.

Bolhar, R., Kamber, B.S., Moorbath, S., Fedo, C.M., Whitehouse, M.J., 2004. Characterization of early Archean chemical sediments by trace element signatures. Earth and Planetary Science Letters 222, 43–60.

Bolhar, R., Van Kranendonk, M.J., Kamber, B.S., 2005. A trace element study of siderite-jasper banded iron formation in the 3.45 Ga Warrawoona Group Pilbara Craton—formation from hydrothermal fluids and shallow water. Precambrian Research 137, 93–114.

Carbonne, J.M., Bard, C.R., Luais, B., 2011. A combined in situ oxygen, silicon isotopic and fluid inclusion study of a chert sample from Onverwacht Group (3.35 Ga South Africa): new constraints on fluid circulation. Chemical Geology 285, 50–61.

Chang, H.J., Chu, X.L., Feng, L.J., et al., 2010. Iron speciation in cherts from the Laobao Formation South China: implications for anoxic and ferruginous deep-water conditions. Chinese Science Bulletin 55, 3189–3196.

Chang, H.J., Chu, X.L., Feng, L.J., 2008. REE geochemistry of the Liuchapo chert in Anhua, Hunan. Geology in China 35, 879–887 (in Chinese with English abstract).

Chen, D.Z., Wang, J.G., Qing, H.R., Yan, D.T., Li, R.W., 2009. Hydrothermal venting activities in the Early Cambrian South China: petrological, geochronological and stable isotopic constraints. Chemical Geology 258, 168–181.

Coplen, T.B., Bohlke, J.K., De Biévre, P., Ding, T.P., Holden, N.E., Hoppl e, J.A., Krouse, H.R., Lamberty, A., Peiser, H.S., Revesz, K., Rieder, S.E., Rosman, K.J.R., Roth, E., Taylor, P.D.P., Vocke, R.D., Xiao, Y.K., 2002. Isotope-abundance variations of selected elements. IUPAC Technical Report. Pure and Applied Chemistry 74, 1987–2017.

Danielson, A., Molller, P., Dulski, P., 1992. The europium anomalies in banded iron formations and the thermal history of the oceanic crust. Chemical Geology 97, 89–100.

De La Rocha, C.L., 2003. Silicon isotope fractionation by marine sponges and the reconstruction of the silicon isotope composition of ancient deep water. Geology 31, 423–426.

De La Rocha, C.L., Bickle, M.J., 2005. Sensitivity of silicon isotopes to whole-ocean changes in the silica cycle. Marine Geology 217, 267–282.
De La Rocha, C.L., Brzezinski, M.A., Deniro, M.J., 1997. Fractionation of silicon isotopes by marine diatoms during biogenic silica formation. Geochimica et Cosmochimica Acta 61, 5051–5056.
Delstanche, S., Opfergelt, S., Cardinal, D., Elsass, F., Andre, L., Delvaux, B., 2009. Silicon isotopic fractionation during adsorption of aqueous monosilicic acid onto iron oxide. Geochimica et Cosmochimica Acta 73, 923–934.
Ding, T.P., et al., 1996. Silicon Isotopes Geochemistry. Geological Publishing House, Beijing (in Chinese).
Ding, T.P., Wan, D.F., Wang, C., 2004. Silicon isotope compositions of dissolved silicon and suspended matter in the Yangtze River, China. Geochimica et Cosmochimica Acta 68, 205–216.
Ding, T.P., Tian, S.H., Sun, L., Wu, L.H., Zhou, J.X., Chen, Z.Y., 2008. Silicon isotope fractionation between rice plants and nutrient solution and its significance to the study of the silicon cycle. Geochimica et Cosmochimica Acta 72, 5600–5615.
Doblas, M., Lopez-Ruiz, J., Cebria, J.M., Youbi, N., Degroote, E., 2002. Mantle insulation beneath the West African craton during the Precambrian–Cambrian transition. Geology 30, 839–842.
Douthitt, C.B., 1982. The geochemistry of the stable isotopes of silicon. Geochimica et Cosmochimica Acta 46, 1449–1458.
Farquhar, J., Bao, H.M., Thiemens, M., 2000. Atmospheric influence of earth's earliest sulfur cycle. Science 289, 756–758.
Fitoussi, C., Bourdon, B., Kleine, T., Oberli, F., Reynolds, B.C., 2009. Si isotope systematics of meteorites and terrestrial peridotites: implications for Mg/Si fractionation in the solar nebula and for Si in the Earth's core. Earth and Planetary Science Letters 287, 77–85.
Friend, C.R.L., Nutman, A.P., Bennett, V.C., Norman, M.D., 2008. Seawater-like trace element signatures (REE + Y) of Eoarchaean chemical sedimentary rocks from southern West Greenland, and their corruption during high-grade metamorphism. Contributions to Mineralogy and Petrology 155, 229–246.
Georg, R.B., Reynolds, B.C., West, A.J., Burton, K.W., Halliday, A.N., 2007. Silicon isotope variations accompanying basalt weathering in Iceland. Earth and Planetary Science Letters 261, 476–490.
Guo, Q.J., Shields, G.A., Liu, C.Q., Strauss, H., Zhu, M.Y., Pi, D.H., Goldberg, T., Yang, X.L., 2007. Trace element chemostratigraphy of two Ediacaran–Cambrian successions in South China: implications for organosedimentary metal enrichment and silicification in the early Cambrian. Palaeogeography, Palaeoclimatology, Palaeoecology 254, 194–216.
Heck, P.R., Huberty, J.M., Kita, N.T., Ushikubo, T., Kozdon, R., Valley, J.W., 2011. SIMS analyses of silicon and oxygen isotope ratios for quartz from Archean and Paleoproterozoic banded iron formations. Geochimica et Cosmochimica Acta 75, 5879–5891.
Herzig, P.M., Becker, K.P., Stoffers, P., Bäcker, H., Blum, N., 1988. Hydrothermal silica chimney fields in the Galapagos Spreading Center at 86°W. Earth and Planetary Science Letters 89, 261–272.
Hren, M.T., Tice, M.M., Chamberlain, C.P., 2009. Oxygen and hydrogen isotope evidence for a temperate climate 3.42 billion years ago. Nature 462, 205–208.
Jacquet, S.H.M., Dehairs, F., Elskens, M., Savoye, N., Cardinal, D., 2007. Barium cycling along WOCE SR3 line in the Southern Ocean. Marine Chemistry 106, 33–45.
Jiang, S.Y., Pi, D.H., Heubeck, C., Frimmel, H., Liu, Y.P., Deng, H.L., Ling, H.F., Yang, J.H., 2009. Early Cambrian ocean anoxia in South China. Nature 459, E5–E6.
Jiang, S.Y., Yang, J.H., Ling, H.F., Feng, H.Z., Chen, Y.Q., Chen, J.H., 2003. Trace- and rare earth element geochemistry and Pb–Pb dating of black shales and intercalated Ni–Mo–PGE–Au sulfide ores in Lower Cambrian strata, Yangtze Platform, South China. Mineralium Deposita 41, 453–468.
Jiang, Y.H., Li, S.R., 2005. A study of the fluid environment of silicalite of transitional Precambrian-Cambrian age in Hunan and Guizhou provinces. Earth Science Frontiers 12, 622–629 (in Chinese with English abstract).
Kirschvink, J.L., Ripperdan, R.L., Evans, D.A., 1997. Evidence for a large-scale reorganization of Early Cambrian continental masses by inertial interchange true polar wander. Science 277, 541–545.
Knauth, L.P., 1994. Petrogenesis of chert. Silica: physical behavior, geochemistry and materials applications. Reviews in Mineralogy 29, 233–258.
Li, S.R., Gao, Z.M., 1996. Silicalite of hydrothermal origin in the Lower Cambrian black rock series of South China. Acta Mineralogica Sinica 16, 416–422 (in Chinese with English abstract).
Li, X.H., 1999. U–Pb zircon ages of granites from the southern margin of the Yangtze Block: timing of Neoproterozoic Jinning Orogeny in SE China and implication for Rodinian assembly. Precambrian Research 97, 45–57.
Li, Y.Y., 1997. The geological characteristics of seafloor exhalative sedimentary chert in the Lower Cambrian-black shales in Dayong-Cili area, Hunan Province. Acta Petrologica Sinica 13, 121–126 (in Chinese).
Li, Y.H., Wan, D.F., Jiang, S.Y., 1995. Silicon isotope study on the Meishucun Precambrian-Cambrian boundary section, Yunnan. Geological Review 41, 179–187 (in Chinese with English abstract).
Lott, D.A., Conveney Jr., R.M., Murowichick, J.B., Grauch, R.I., 1999. Sedimentary exhalative nickel–molybdenum ores in south China. Economic Geology and the Bulletin of the Society of Economic Geologists 94, 1051–1066.
Lott, D.A., Coveney Jr., R.M., 1996. Fluid-inclusion evidence for the origins of organic-rich Chinese nickel–molybdenum ores. In: Abstracts of 30th IGC, vol. 2, Beijing, p. 713.
Luo, T.Y., Ning, X.X., Luo, Y.L., Li, X.B., Ling, R.X., Yao, L.B., 2005. Super-enrichment of Se in the bottom black shales Lower Cambrian at Zunyi, Guizhou province, China. Acta Mineralogica Sinica 25, 275–282 (in Chinese with English abstract).
Mao, J.W., Lehmann, B., Du, A.D., Zhang, G.D., Ma, D.S., 2002. Re-Os dating of polymetallic Ni-Mo-PGE-Au mineralization in Lower Cambrian black shales of South China and its geologic significance. Economic Geology 97, 1051–1061.
Michard, A., Albarede, F., Michard, G., Minster, j., charlou, f.J., 1983. Rare-earth elements and uranium in high-temperature solutions from East Pacific Rise hydrothermal vent field (13°N). Nature 303, 795–797.
Nozaki, Y., Zhang, J., Amakawa, H., 1997. The fractionation between Y and Ho in the marine environment. Earth and Planetary Science Letters 148, 329–340.
Pack, A., Russell, S.S., Shelley, J.M.G., Van Zuilen, M., 2007. Geo- and cosmochemistry of the twin elements yttrium and holmium. Geochimica et Cosmochimica Acta 71, 4592–4608.
Peng, J., Xia, W.J., Yin, H.S., 1999. Geochemical characteristics and depositional environments of late Precambrian bedded siliceous rocks in western Hunan. Sedimentary Facies and Palaeogeography 19, 29–37 (in Chinese with English abstract).
Qi, L., Hu, J., Gregoire, D.C., 2000. Determination of trace elements in granites by inductively coupled plasma mass spectrometry. Talanta 51, 507–513.
Robert, F., Chaussidon, M., 2006. A palaeotemperature curve for the Precambrian oceans based on silicon isotopes in cherts. Nature 443, 969–972.
Savage, P.S., Georg, R.B., Armytage, R.M.G., Williams, H.M., Halliday, A.N., 2010. Silicon isotope homogeneity in the mantle. Earth and Planetary Science Letters 295, 139–146.
Shields, G., Stille, P., 2001. Diagenetic constraints on the use of cerium anomalies as palaeoseawater redox proxies: an isotopic and REE study of Cambrian phosphorites. Chemical Geology 175, 29–48.
Siever, R., 1992. The silica cycle in the Precambrian. Geochimica et Cosmochimica Acta 56, 3265–3272.
Steiner, M., Wallis, E., Ertman, B.D., Zhao, Y.L., Yang, R.D., 2001. Submarine hydrothermal exhalative ore layers in black shales from South China and associated fossils insights into Lower Cambrian facies and bio-evolution. Palaeogeography, Palaeoclimatology, Palaeoecology 169, 165–169.
Stüben, D., Taibi, N.E., McMurtry, G.M., Scholten, J., Stoffers, P., Zhang, D., 1994. Growth history of a hydrothermal silicon chimney from the Marian back-arc spreading center (southwest Pacific, 18°13′N). Chemical Geology 113, 273–296.
Sugahara, H., Sugitani, K., Mimura, K., Yamashita, F., Yamamoto, K., 2010. A systematic rare-earth elements and yttrium study of Archean cherts at the Mount Goldsworthy greenstone belt in the Pilbara Craton: Implications for the origin of microfossil-bearing black cherts. Precambrian Research 177, 73–87.
Sugisaki, R., 1984. Relation between chemical composition and sedimentation rate of Pacific ocean-floor sediments deposited since the middle Cretaceous: basic evidence for chemical constraints on depositional environments of ancient sediments. The Journal of Geology 92, 235–259.
Sverjensky, D.A., 1984. Europium redox equilibria in aqueous solution. Earth and Planetary Science Letters 67, 70–78.
Turekian, K.K., Wedepohl, K.H., 1961. Distribution of the elements in some major units of the earth's crust. Geological Society of America Bulletin 72, 175–192.
Van den Boorn, S.H.J.M., van Bergen, M.J., Nijman, W., Vroon, P.Z., 2007. Dual role of seawater and hydrothermal fluids in Early Archean chert formation: evidence from silicon isotopes. Geology 35, 939–942.
Van den Boorn, S.H.J.M., van Bergen, M.J., Vroon, P.Z., de Vries, S.T., Nijman, W., 2010. Silicon isotope and trace element constraints on the origin of 3.5 Ga cherts: implications for Early Archean marine environments. Geochimica et Cosmochimica Acta 74, 1077–1103.
Veevers, J.J., Walter, M.R., Schneiber, E., 1997. Neoproterozoic tectonics of Australia Antarctic and Laurentia and the 560 Ma birth of the Pacific Ocean reflect the 400 my. Pangean Supercycle. The Journal of Geology 105, 225–242.
Von Damm, K.L., Bischoff, J.L., Rosenbauer, R.J., 1991. Quartz solubility in hydrothermal seawater: an experimental study and equation describing quartz solubility for up to 0.5 M NaCl solutions. American Journal of Science 291, 977–1007.
Wang, D.A., Chen, R.J., 1996. Discussion on silicon isotope of bedded siliceous rocks of different ages in Yangtze Platform. Acta Sendimentologica Sinica 14, 82–88 (in Chinese with English abstract).
Wang, J., Li, Z.X., 2003. History of Neoproterozoic rift basins in South China: implications for Rodinia break-up. Precambrian Research 122, 141–158.
Yamamoto, K., 1987. Geochemical characteristics and depositional environments of cherts and associated rocks in the Franciscan and Shimanto Terranes. Sedimentary Geology 52, 65–108.
Yang, A., Zhu, M., Zhang, J., Li, G., 2003. Early Cambrian eodiscoid trilobites of the Yangtze Platform and their stratigraphic implications. Progress in Natural Science 13, 861–866.
Yang, R.D., Wei, H.R., Bao, M., Wang, W., Wang, Q., Zhang, X.D., Liu, L., 2008. Discovery of hydrothermal venting community at the base of Cambrian barite in Guizhou Province Western China: implication for the Cambrian biological explosion. Progress in Natural Science 18, 65–70.
Zhang, J., Zhu, M., Yang, A., et al., 2004. Stratigraphic implications of Sinian to Early Cambrian volcanic ash beds on the Yangtze Platform. Progress in Natural Science 14, 72–76.
Zheng, Y.F., Wu, R.X., Wu, Y.B., Zhang, S.B., Yuan, H.L., Wu, F.Y., 2008. Rift melting of juvenile arc-derived crust: geochemical evidence from Neoproterozoic volcanic

and granitic rocks in the Jiangnan Orogen, South China. Precambrian Research 163, 351–383.
Zhou, M.Z., Luo, T.Y., Li, Z.X., Zhao, H., Long, H.S., Yang, Y., 2008. SHRIMP U–Pb zircon age of tuff at the bottom of the Lower Cambrian Niutitang Formation, Zunyi, South China. Chinese Science Bulletin 53, 4576–4583.
Ziegler, K., Chadwick, O.A., Brzezinski, M.A., Kelly, E.F., 2005. Natural variations of d30Si ratios during progressive basalt weathering, Hawaiian Islands. Geochimica et Cosmochimica Acta 69, 4597–4610.